

Article

The Impacts of the Hydrological Regime on the Soil Aggregate Size Distribution and Stability in the Riparian Zone of the Three Gorges Reservoir, China

Shujuan Zhang ¹, Tianyi Chen ¹, Yuhai Bao ² , Qiang Tang ³, Yongtao Li ^{1,*} and Xiubin He ^{2,*}

¹ College of Natural Resources and Environment, Joint Institute for Environmental Research & Education, South China Agricultural University, Guangzhou 510642, China

² Key Laboratory of Mountain Surface Processes and Ecological Regulation, Institute of Mountain Hazards and Environment, Chinese Academy of Sciences, Chengdu 610041, China

³ Chongqing Jinpo Mountain Karst Ecosystem National Observation and Research Station, School of Geographical Sciences, Southwest University, Chongqing 400715, China

* Correspondence: yongtao@scau.edu.cn (Y.L.); xiubinh@imde.ac.cn (X.H.)

Abstract: The impoundment of the Three Gorges Reservoir (TGR) has greatly altered the hydrological regime and thus formed a distinctive riparian zone with anti-seasonal inundation and exposure, which may affect the soil aggregate properties in this riparian zone. Yet, the soil aggregate size distribution and stability influenced by the hydrological regime along the step-impounded elevation have rarely been documented. This study aimed to elucidate how the hydrological regime of the TGR affected the aggregate size distribution and stability in the riparian zone. Based on the step-impounded elevation, topsoil samples were collected from four elevation-dependent transects in a middle section of the TGR. Dry-sieving and wet-sieving methods were employed. The results showed that, with a decrease in the elevation gradient, the mass percentage of the >5 mm aggregates significantly decreased, while the proportions of the other size classes presented an increasing trend. Additionally, the mean weight diameter (MWD), geometric mean diameter (GMD), aggregate stability rate (ASR), and percentage of aggregate destruction (PAD) of the fractal dimension showed a successive decrease with a decrease in the elevation gradient, whereas PAD_{MWD}, PAD_{GMD}, PAD_{ASR}, and the fractal dimension demonstrated a reverse trend. It can thus be deduced that the hydrological regime of the TGR significantly modified the aggregate size distribution and dramatically reduced the aggregate stability, which may provide a crucial basis for assessing the soil erosion in similar riparian zones.

Keywords: aggregate size distribution; aggregate stability; wetting and drying cycles; hydrological regime; Three Gorges Reservoir



Citation: Zhang, S.; Chen, T.; Bao, Y.; Tang, Q.; Li, Y.; He, X. The Impacts of the Hydrological Regime on the Soil Aggregate Size Distribution and Stability in the Riparian Zone of the Three Gorges Reservoir, China. *Water* **2023**, *15*, 1791. <https://doi.org/10.3390/w15091791>

Academic Editors: Achim A. Beylich, Adimalla Narsimha, Xudong Peng and Lunjiang Wang

Received: 11 February 2023

Revised: 17 April 2023

Accepted: 4 May 2023

Published: 7 May 2023



Copyright: © 2023 by the authors. Licensee MDPI, Basel, Switzerland. This article is an open access article distributed under the terms and conditions of the Creative Commons Attribution (CC BY) license (<https://creativecommons.org/licenses/by/4.0/>).

1. Introduction

Soil structure is a fundamental property that controls various soil processes (e.g., aggregation, sorption, solution, redox, and mineralization) and influences several soil functions (e.g., regulation function, habitat function, and production function) [1]. Soil aggregate, as the basic unit of soil structure, is one of the important soil components that regulates its related processes and functions such as water infiltration, carbon sequestration [2], root penetration, crust formation [3], and surface erosion [4,5]. Aggregate stability refers to the resistance of the soil aggregate against disintegration by external disruptive forces such as water, wind, or managements [6,7]. A higher aggregate stability is beneficial for improving soil fertility, infiltration, anti-erosion, sustainability, and productivity. Consequently, soil aggregate stability is widely considered as a key indicator of soil quality [8] and soil susceptibility to erodibility [9]. Therefore, measuring soil aggregate size distribution and stability under numerous factors is essential to assessing soil erosion risks and providing implications for soil sustainable managements.

Soil aggregate size distribution and stability depend on both internal factors and external factors, with the external factors affecting the aggregate stability by mediating the internal factors [10]. Generally, the wetting and drying (WD) cycle is a key external factor causing strong alterations in the aggregate stability through its direct effects on soil moisture and indirect impacts on soil microorganisms [11]. It is well accepted that the WD cycle is a common phenomenon frequently induced by seasonal climate alternation, irrigation and drainage, or water level fluctuation. Laboratory experiments and field studies have revealed that WD cycles can promote the generation of aggregates in unaggregated soil, but that they produce inconsistent effects on the aggregate stability in aggregated soil [12,13]. Peng et al. [14] found a decrease in aggregate stability with increasing numbers of WD cycles in the non-rigid Gleysols. On the contrary, Rahman et al. [15] reported an improvement in soil aggregation under WD cycles in the Vertisols. Additionally, Cosentino et al. [11] reported that WD cycles showed no, negative, and positive effects on aggregate stability under fast rewetting, slow rewetting, and stirring after a prewetting test in a silt loam soil, respectively. These contradictions in the effects of WD cycles on aggregate stability are closely related to the different intrinsic soil properties (e.g., initial soil moisture, clay mineral, organic matter, exchangeable cations, and aggregate size), as well as the intensity and duration of the WD cycles. Thus, the study of soil aggregate stability under WD cycles has attracted the extensive attention of researchers. However, these studies have mainly focused on agricultural or terrestrial soils affected by rainfall-derived or irrigation-derived WD cycles, and not much attention has been paid to soil aggregate in a reservoir riparian zone, where soil undergoes intensely special WD cycles due to the coexistence of rainfall impacts and water level fluctuation.

Reservoirs represent an artificial disturbance to natural river channels and are designed for hydropower generation, flood control, and navigation improvement, etc. [16]. The impoundment of reservoirs may alter the original hydrological regimes, thus arousing environmental issues such as soil structure degradation [17], biodiversity reduction, soil erosion [18,19], sediment deposition [20], and bank instability. Particularly, the Three Gorges Reservoir (TGR) in the People's Republic of China is a well-known reservoir that is formed by the operation of the Three Gorges Dam, the largest hydropower project in the world. The TGR carried out step-by-step impoundment with an elevation of 135 m in 2003, subsequently increasing to 156 m, 172 m, and 175 m in 2006, 2008, and 2010, respectively [21]. Since 2010, the water level has annually fluctuated between 145 m and 175 m, leading to the formation of a riparian zone in the TGR. A riparian zone is a transitional zone between the base level and peak level, suffering from seasonal submergence and exposure via water level fluctuation and rainfall. Compared to other reservoir riparian zones, the riparian zone of the TGR is a unique geomorphological unit with a larger extent, greater height, and anti-seasonal hydrological regime [21]. Longitudinally, it extends 663 km from Jiangjin, Chongqing City to Yichang, Hubei Province, with a total area of 349 km². Laterally, it covers a vertical height of 30 m from 145 m to 175 m. Temporally, its water level fluctuates anti-seasonally between the base level of 145 m during the wet season (May to September) and the peak level of 175 m during the dry season (October to April), suggesting that the winter flooding regime of the TGR is opposite to the seasonal summer flooding regime of the natural river. Besides its anthropogenic-regulated water level fluctuation, its altered hydrological regime is also influenced by rainfall and waves, reflecting a variable flooding regime (e.g., flooding timing, magnitude, frequency, intensity, and duration) along its elevation gradient. These changes have resulted in highly spatial–temporal heterogeneities in the geomorphological, geochemical, and ecological processes that interact with the diverse bedrocks, soil types, topography, vegetation species, and human activities in the riparian zone of the TGR [21].

Specifically, riparian soils experience annual WD cycles with seasonal submergence and exposure caused by water level fluctuation and rainfall, which finally alter the soil aggregate composition and stability. During the submerged or rainfall process, the water level rapidly increases, resulting in the swelling of soil particles and the disintegration of

soil aggregates [22]. During the exposed phase, the capillary forces, surface tension forces, and soil cohesive forces change with continued drying, resulting in the shrinkage of soil particles and the formation of cracks [23]. However, soils exhibit non-uniformity swelling and shrinking with irreversible volumetric deformation [24,25], which is responsible for the altered aggregate size distribution. Nsabimana et al. [5] reported a tremendous decline in the mass proportion of >5 mm aggregates and a dramatic rise in the mass proportion of <0.25 mm aggregates with an increasing wet shaking frequency for the riparian soil, whilst Ran et al. [26] revealed that the highest and lowest proportions of >2 mm large macro-aggregates were present in the intermediate and weak hydrological stress, and those of 0.25–2 mm small macro-aggregates were shown in the weak and strong hydrological stresses, respectively. As for the soil aggregate stability, Ran et al. [26,27] demonstrated that this aggregate stability was the highest and the lowest under the intermediate and strong hydrological stresses, respectively, whilst Cui et al. [17] observed that the aggregate stability was highest and lowest under the none and intermediate hydrological stresses. Moreover, Nsabimana et al. [28] concluded that the stability of the aggregates less than 2 mm decreased as the elevation increased, using laser diffraction method, while he pointed out that the aggregate stability increased as the elevation increased, using wetting and wet-shaking methods [29]. The above mentioned studies have presented discrepancies in the effects of the hydrological regime on soil aggregates in the riparian zone. Since soil aggregate size distribution and stability may be heterogeneous at different spatial and temporal scales in the riparian zone, this can contribute to the advancement of knowledge on soil aggregates in the riparian zone, in order to elaborate upon the impacts of hydrological regimes on soil aggregates. Furthermore, considering the 30 m vertical height of the water level fluctuation in the riparian zone, previous studies have investigated the soil aggregate properties at equal intervals of 5 m or 10 m along the elevation gradient. However, few studies have been conducted to evaluate the soil aggregate based on the step-impounded elevation of the TGR. We thus hypothesized that the hydrological regime could modify the aggregate size distribution and stability. To test our hypothesis, we employed dry-sieving and wet-sieving methods to investigate the characteristics of the aggregate size distribution and stability along the step-impounded elevation in a typical section of the TGR riparian zone. The specific objective of the present study was to evaluate the changes in the aggregate size distribution and stability along the elevation gradient as a means of assessing the effects of variations in the hydrological regime on soil aggregate stability.

2. Materials and Methods

2.1. Study Area

The riparian zone of the TGR is a transitional zone formed by its hydrological regime and it contains 26 administrative units from Chongqing to Yichang along the Upper Yangtze River (Figure 1). The present study was conducted on the left bank of a central section of the riparian zone along the Yangtze mainstream, located in Zhong County, Chongqing City (107°32′–108°14′ E, 30°03′–30°35′ N) (Figure 1). The area is characterized by a hilly landscape and low mountains with gentle slope gradients of less than 15°. The climate belongs to a humid, subtropical monsoon climate with a mean annual temperature of 18.2 °C and an average annual precipitation of 1172.1 mm, which predominantly falls in the rainy season from May to September. The bedrocks are defined as purple and red rocks composed of sandstones and mudstones from the Jurassic Shaximiao Group (J2s) [17]. The widely distributed soil in the area is locally known as “purple soil” (Genetic Soil Classification of China), which is classified as Entisol in the USDA Taxonomic System [30]. As the “purple soil” has a loamy soil texture with strong physical weathering and a poor water stability, it is susceptible to soil erosion. The previous landform before the reservoir impoundment consisted of arable lands and grassland, which have been transformed into grassland and bare land after the impoundment of the TGR. The vegetation in the study area is dominated by annual plants (e.g., *Xanthium sibiricum* and *Digitaria sanguinalis*)

and perennial herbs (*Cynodon dactylon*, *Hemarthria altissima*, *Paspalum paspaloides*, and *Alternanthera philoxeroides*) [31].

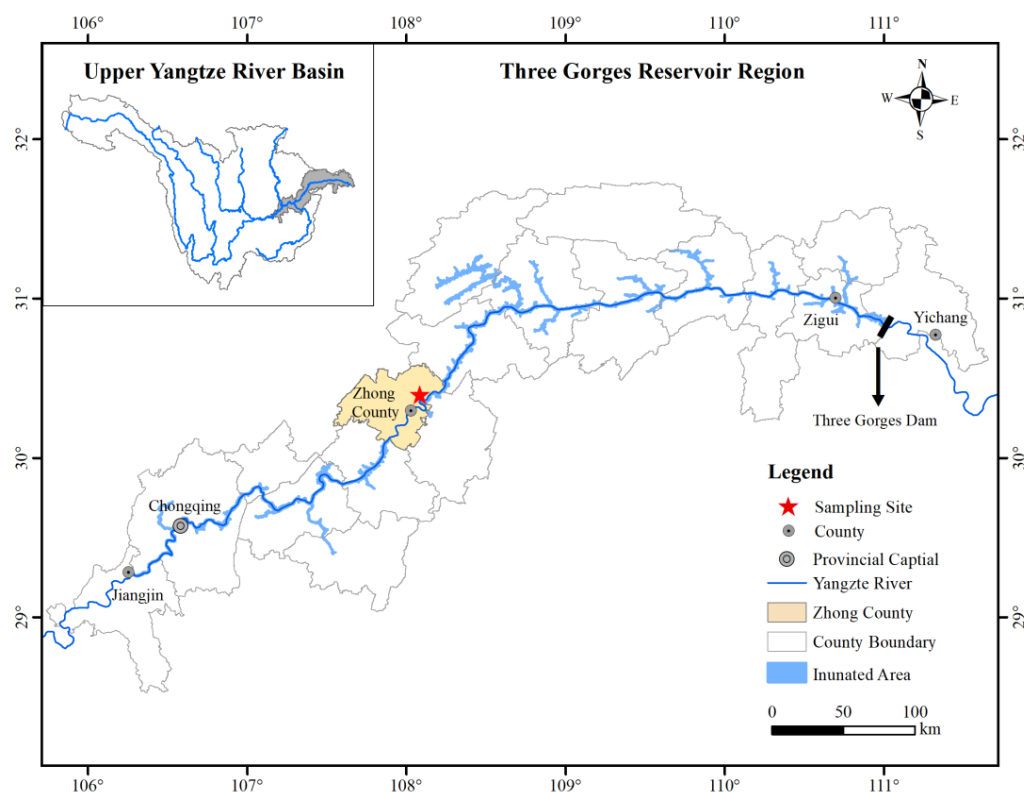


Figure 1. Location of the Three Gorges Reservoir and the sampling site.

2.2. Field Sampling

The field sampling was carried out in September 2016 when the water level stayed at around 146 m and the riparian zone was extensively exposed. Since the hydrological regime of the riparian zone is characterized by an annual artificial flow regulation between 145 m and 175 m, combined with additional changes caused by frequent rainfall events during the wet season (Figure 2a), the hydrological regime (e.g., inundation year, frequency, duration, and magnitude) was diverse along the elevation gradient. Considering that the hydrological regime was operated by step-by-step impoundment, with increasing magnitudes of 156, 172, and 175 m above sea level in 2006, 2008, and 2010, respectively (Figure 2a), four sampling transects along the elevation gradient were set up in each slope belt, which were labeled as LI (long-term inundation, 145–156 m), MI (moderate inundation, 156–172 m), SI (short-term inundation, 172–175 m), and CK (none inundation, 175–180m), respectively (Figure 2b). The soil samples collected from 175–180 m were considered as controls and the samples from 145–175 m represented riparian soils. Three slope belts, at approximately equal distances at the horizontal interval of 5 m on the mainstream left bank, perpendicular to the water flow direction, were selected as the sampling belts (Figure 2b). All the landscapes of the sampling belts were grassland. The dominant vegetations in CK and SI included *Cynodon dactylon*, *Hemarthria altissima*, *Digitaria sanguinalis*, *Paspalum paspaloides*, and *Xanthium sibiricum*. The prevailing vegetations in MI consisted of *Cynodon dactylon*, *Paspalum paspaloides*, *Xanthium sibiricum*, and *Digitaria sanguinalis*. The vegetations in LI were dominated by *Cynodon dactylon* and *Alternanthera philoxeroides*. The other basic information on these sampling transects is presented in Table 1.

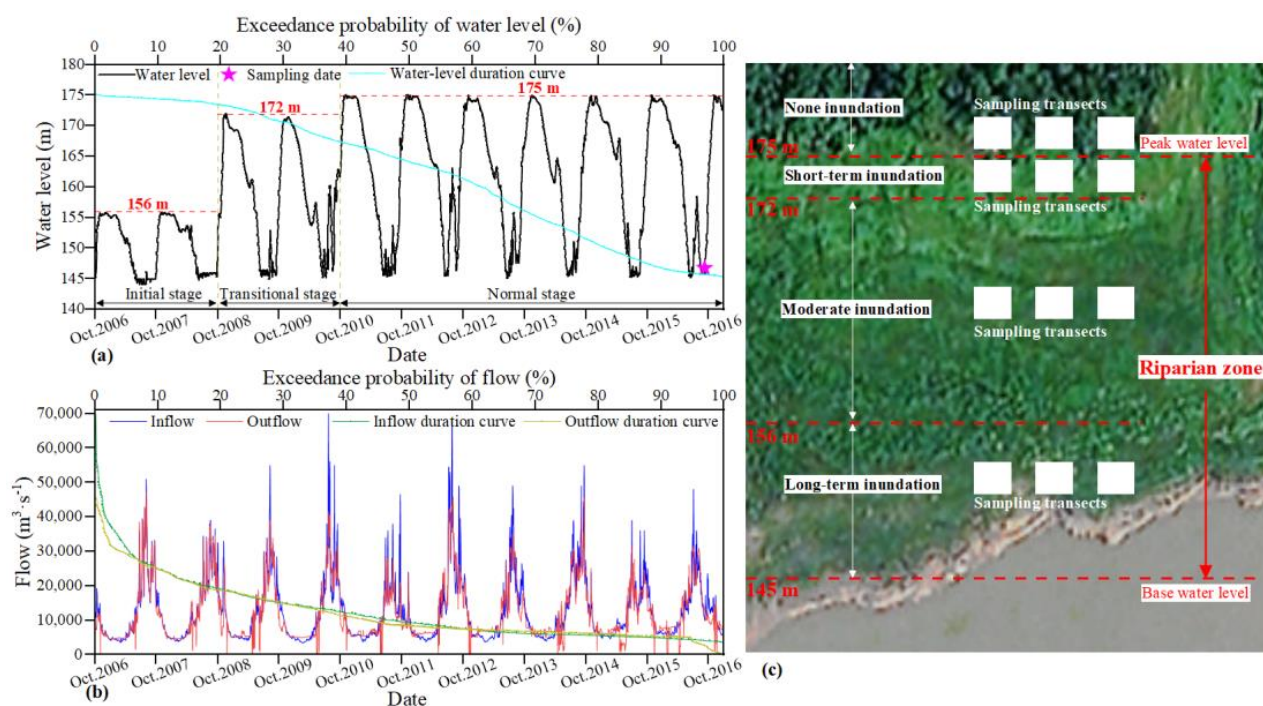


Figure 2. The water level hydrograph and water level duration curve in the Three Gorges Reservoir (a); the flow hydrograph and flow duration curve in the Three Gorges Reservoir (b); and schematic diagram of sampling design (c). Data on reservoir water level and flow were obtained from the China Three Gorges Corporation (<http://www.ctg.com.cn/>, accessed on 31 December 2016).

Table 1. Basic information on the sampling transects along the elevation gradient in the riparian zone of the Three Gorges Reservoir.

Sampling Transects	Inundation Year (Year)	Inundation Month	Inundation Day (Day)	Inundation Height (m)	Soil Type	Vegetation Cover (%)	Slop Gradient (°)
CK	0	0	0	0	Entisol	72	3–5
SI	6	October–January	3–97	0–3	Entisol	70	3–5
MI	8	September–April	97–249	3–19	Entisol	67	4–7
LI	10	September–May	249–365	19–30	Entisol	63	5–9

Note: CK (none inundation, 175–180m); SI (short-term inundation, 172–175 m); MI (moderate inundation, 156–172 m); and LI (long-term inundation, 145–156 m).

For determining the aggregate size distribution and stability, three undisturbed topsoil clods of 10 × 10 × 10 cm were collected with a shovel after removing the residues, weeds, and deposited sediments in each transect. Following this, the samples were put into a plastic box. In each transect, three undisturbed topsoil cores (5 cm in length and 5 cm in diameter) were also, respectively, collected from both the 0–5 cm and 5–10 cm layers using the cutting ring for testing the bulk density. The bulk density in each transect was determined as the mean value of the two-layer bulk density. The bulk topsoil samples (0–10 cm) were collected using a shovel from four corners and the center in each transect and then evenly mixed into a composite sample (2 kg in weight) that was sealed in a single zip-lock bag for measuring the particle size distribution, pH, and organic carbon content. A total of 36 undisturbed topsoil blocks, 72 undisturbed topsoil cores, and 36 composite samples were carefully taken back to the laboratory for the next analysis.

2.3. Soil Properties Analysis

The composite samples were air dried at room temperature in the laboratory. Then, each composite sample was ground to pass through 2 mm and 0.25 mm sieves for deter-

mining the basic soil properties (e.g., soil texture, soil pH, organic carbon, and particle density). The soil particle size distribution was measured using a laser particle size analyzer (Mastersizer 2000, Malvern Instruments Ltd., Worcestershire, UK). Before the measurement was taken, 0.5 g of soil that had passed through the 2 mm sieve was taken from each sample and placed into a 25 mL beaker. Next, a 5 mL sodium hexametaphosphate dispersion solution was added to the beaker, followed by the addition of 15 mL of distilled water. Then, the beaker was shaken for 1–2 h. Subsequently, the Mastersizer 2000 with one sample dispersion unit was initiated to take a measurement. The sample concentration was controlled by monitoring the obscuration of the laser beam caused by the sample being added to the dispersant. In the present study, deionized water was used as the dispersant and the prepared soil sample was gradually added to a beaker with 1000 mL of deionized water until the obscuration was in the range of 10–20%. Finally, the raw data on the soil particle size distribution were supplied by the Malvern software in the Mastersizer 2000. Based on the United States Department of Agriculture's classification system, soil particle sizes of less than 2 μm , 2–50 μm , and 50–2000 μm were classified as clay, silt, and sand, respectively. A pH meter (model cyberscan 510, Singapore) was applied to test the soil pH at a soil: water ratio of 1:2.5. The soil organic carbon was determined with an element analyzer (vario EL, Elementar Analyser System GmbH, Hanau, Germany). The liquid pycnometer method was used to measure the particle density (Soil Survey Laboratory Methods Manual, 2004). Additionally, the bulk density of the undisturbed soil core was obtained using the cutting ring method and calculated using the mass of the oven-dried soil divided by the volume of the cutting ring. The total porosity was calculated using the equation based on the relationship between the bulk density and particle density (Soil Survey Laboratory Methods Manual, 2004).

2.4. Soil Aggregate Analysis

The undisturbed soil cores were used for detecting the aggregate distribution and stability. The soil cores were first broken into small parts around 10 mm along their natural fissures by hand. Then, the broken samples were air dried at room temperature after manually removing any residues and debris in the laboratory. The air-dried samples were tested by both dry-sieving and wet-sieving methods, as proposed by Yoder [32] and Kemper and Rosenau [33]. Briefly, to measure the mechanical-stable aggregate size distribution, five hundred grams of each soil sample was placed in the top of a nest of five sieves with descending aperture of 5, 2, 1, 0.5, and 0.25 mm. Then, the sample was shaken for 10 min with a reciprocating shaker (Retsch VS. 1000) at the speed of 250 r/min. After this process, the soil aggregates remaining on each sieve were weighted and the mass percentages of six fractions (>5 mm, 5–2 mm, 2–1 mm, 1–0.5 mm, 0.5–0.25 mm, and <0.25 mm) were calculated. Subsequently, to determine the water-stable aggregate distribution, four composite subsamples (50 g for each subsample) were gained from each sample by proportionally mixing the six fractions according to the corresponding mass percentages described above. Then, each composite subsample was put in the top of the stacking sieves (5, 2, 1, 0.5, and 0.25 mm) in an aggregate analyzer, which comprised four independent and identical cylindrical water containers [34]. Following this, the nest of five sieves was stabilized in the analyzer and surrounded by water containers. Following this, the distilled water was poured into the water containers until the topmost sieve did not exceed the water surface when it was at its highest. After the soil subsample was immersed in water for 10 min, the analyzer worked for 30 min with a frequency of 30 r/min and a vertical amplitude of 4 cm. Then, the nest was slowly raised to leave the water surface and the aggregates retained on each sieve were, respectively, washed into boxes with distilled water. Once the solution in the boxes was clarified, the clear water on the upper part was poured out. Finally, the aggregates remaining in the boxes were oven dried and subsequently weighted. Each aggregate sample was measured through 4 parallel subsamples and the results were taken as the arithmetic mean values.

The aggregate stability was evaluated by the indicators of mean weight diameter (MWD) [35], geometric mean diameter (GMD) [36], aggregate stability rate (ASR), fractal dimension (D) [37], and the percentage of aggregate destruction (PAD) [38]. The higher the MWD, GMD, and ASR values, the stronger aggregate stability, whilst the higher the resulting PAD_{MWD} , PAD_{GMD} , and PAD_{ASR} values, the weaker aggregate stability. In contrast, the larger the D value, the weaker aggregate stability, while this is the opposite for the PAD_D . Detailed equations for the related indicators are presented below:

$$MWD = \sum_1^n X_i \times \frac{m_i}{m}, \quad (1)$$

$$PAD_{MWD} = \frac{MWD_d - MWD_w}{MWD_d} \times 100\% \quad (2)$$

$$GMD = \exp \left[\sum_{i=1}^n m_i \log X_i / m \right], \quad (3)$$

$$PAD_{GMD} = \frac{GMD_d - GMD_w}{GMD_d} \times 100\% \quad (4)$$

$$ASR = m_j / m \times 100\%, \quad (5)$$

$$PAD_{ASR} = \frac{ASR_d - ASR_w}{ASR_d} \times 100\%, \quad (6)$$

$$D = 3 - \frac{\lg(w_i / m)}{\lg(X_i / X_{max})}, \quad (7)$$

$$PAD_D = \frac{D_w - D_d}{D_d} \times 100\% \quad (8)$$

where X_i is the mean aperture of the adjacent i and $i + 1$ sieves; n is the number of sieves; m_i is the mass of the aggregates on the i th sieve; m is the total mass of the aggregates; MWD_d and MWD_w are the mean weight diameters of the dry-sieved and wet-sieved aggregates, respectively; GMD_d and GMD_w are the geometric mean diameters of the dry-sieved and wet-sieved aggregates, respectively; m_j is the mass of the aggregates larger than 0.25 mm; ASR_d is the mass proportion of the dry-sieved aggregates larger than 0.25 mm; ASR_w is the mass proportion of the wet-sieved aggregates larger than 0.25 mm; w_i is the mass of the aggregates with a size less than X_i ; X_{max} is the mean diameter of the aggregates at the top sieve; and D_d and D_w are the fractal dimensions of the dry-sieved and wet-sieved aggregates, respectively.

2.5. Statistical Analysis

The data were processed using Microsoft Excel software (Version 2016) and the figures were drawn using Origin software (Version 2022, OriginLab Corporation). The significant differences in the soil properties and aggregate stability along the elevation gradient were determined using one-way analyses of variance (ANOVA). The statistical analysis was performed with the least significant difference method (LSD) at a significance level of $p < 0.05$. A Pearson correlation analysis was used to evaluate the relationships between the soil basic properties and aggregate stability. All the statistical analyses were performed with SPSS software (Version 26, IBM SPSS Inc., Chicago, IL, USA).

3. Results

3.1. Soil Physical and Chemical Properties

The soil basic physicochemical properties of the sampling transects are shown in Table 2. Although the soils at the four sampling transects were all classified as loamy

soils, the soils were more and more coarse textured with a decrease in the elevation gradient. Compared to the referenced soils in upland hillslopes (CK), the sand fraction of the riparian soils (i.e., SI, MI, and LI), influenced by the hydrological regime of the TGR, significantly increased by 186.46%, 103.89%, and 26.39%, while the silt fraction decreased by 1.89%, 9.11%, and 15.85%, and the clay fraction declined by 13.36%, 12.42%, and 34.22%, respectively. With a decrease in the elevation gradient, the bulk densities increased from $1.26 \text{ g}\cdot\text{cm}^{-3}$ in CK to $1.56 \text{ g}\cdot\text{cm}^{-3}$ in LI, while the total porosity revealed a reduction from 52.31% in CK to 41.00% in LI. The soils were alkaline with pH values ranging from 8.19 to 8.59. The bulk density, total porosity, and pH were significantly different between the soils in the upland hillslopes and the soils in the riparian zone ($p < 0.05$), whilst the differences were not statistically significant among the three sampling transects within the riparian zone ($p > 0.05$). The soil organic carbon (SOC) was significantly different among the four sampling transects and it reflected a dramatic dwindling of $2.03 \text{ g}\cdot\text{kg}^{-1}$, $4.23 \text{ g}\cdot\text{kg}^{-1}$, and $8.43 \text{ g}\cdot\text{kg}^{-1}$ in the riparian soils of SI, MI, and LI in comparison to CK, respectively. These results suggested that the hydrological regime of the TGR varied in the soil basic properties of the riparian zone, and that the modification of the SOC was particularly prominent.

Table 2. Soil physicochemical properties of the sampling transects along the elevation gradient in the riparian zone of the TGR.

Sampling Transects	Sand (%)	Silt (%)	Clay (%)	BD ($\text{g}\cdot\text{cm}^{-3}$)	Total Porosity (%)	pH	SOC ($\text{g}\cdot\text{kg}^{-1}$)
CK	8.17 ± 0.81 c	88.18 ± 0.44 a	3.65 ± 0.43 a	1.26 ± 0.21 b	52.31 ± 8.08 a	8.19 ± 0.05 b	12.59 ± 1.51 a
SI	10.32 ± 0.63 c	86.52 ± 0.45 a	3.16 ± 0.19 a	1.42 ± 0.12 a	46.23 ± 4.65 b	8.59 ± 0.06 a	10.56 ± 1.22 b
MI	16.65 ± 2.90 b	80.15 ± 2.86 b	3.20 ± 0.25 a	1.49 ± 0.15 a	43.65 ± 5.49 b	8.55 ± 0.24 a	8.36 ± 1.06 c
LI	23.39 ± 5.56 a	74.21 ± 4.93 c	2.40 ± 0.72 b	1.56 ± 0.13 a	41.00 ± 4.95 b	8.59 ± 0.05 a	4.16 ± 0.99 d

Note: CK (none inundation, 175–180 m); SI (short-term inundation, 172–175 m); MI (moderate inundation, 156–172 m); and LI (long-term inundation, 145–156 m). Sand (0.05–2 mm); silt (0.002–0.05 mm); and clay (<0.005 mm). BD, bulk density. SOC, soil organic carbon. Values are means \pm standard deviations ($n = 9$). Different letters (a, b, c, and d) in each column indicate significant differences among the four sampling transects at the $p < 0.05$ level (LSD).

3.2. Size Distribution of Mechanically Stable Aggregates

Using the dry-sieving method, we found that the hydrological regime changed the size distribution of the mechanically stable aggregates (Table 3). The mechanically stable aggregates at the four sampling transects were all dominated by macro-aggregates (i.e., aggregates greater than 0.25 mm), particularly by aggregates larger than 5 mm with a percentage varying between 63.55% and 79.15%. Compared to the soil aggregates in CK, the mass percentages of the >5 mm fractions in HI, MI, and LI were significantly decreased by 10.64%, 11.71%, and 18.82%, while those of the other five fractions in HI, MI, and LI showed an apparent increasing trend. As for the 5–2 mm aggregates, significant differences only appeared between LI and CK, which had the highest mass percentage (17.90%) and lowest mass percentage (13.28%), respectively. In terms of the 2–1 mm and 1–0.5 mm aggregates, the mass percentages in the riparian zone significantly changed, with average increases of 69.83% and 112.43% in comparison to those in the upland hillslopes (CK) ($p < 0.05$), whilst the percentages were insignificantly different among the three sampling transects within the riparian zone ($p > 0.05$). Additionally, the mass percentage of the 0.5–0.25 mm aggregates revealed an increasing trend in the order of CK < LI < SI < MI. With a decrease in the elevation gradient, the mass fraction of the <0.25 mm micro-aggregates increased by 63.64%, 149.22%, and 288.18%, and a significant difference appeared between LI and CK. These changes indicated that the hydrological regime disrupted a great proportion of the larger aggregates into smaller aggregates, and that the transformation was stronger and stronger as the elevation decreased.

Table 3. Differential size distribution of mechanically stable aggregates at four sampling transects in the riparian zone of the TGR.

Sampling Transects	Mass Percentage of Aggregates at Different Sizes (%)					
	>5 mm	5–2 mm	2–1 mm	1–0.5 mm	0.5–0.25 mm	<0.25 mm
CK	79.15 ± 3.47 a	13.28 ± 2.24 b	4.31 ± 0.82 b	1.30 ± 0.27 b	0.74 ± 0.13 b	1.22 ± 0.01 b
SI	70.73 ± 1.30 b	15.23 ± 1.76 ab	6.81 ± 0.15 a	2.74 ± 0.13 a	2.49 ± 0.35 ab	2.00 ± 0.14 b
MI	69.87 ± 2.03 b	14.61 ± 0.68 ab	6.89 ± 0.51 a	2.73 ± 0.27 a	2.85 ± 0.45 a	3.05 ± 0.57 ab
LI	64.25 ± 1.24 b	17.90 ± 0.54 a	8.26 ± 0.44 a	2.82 ± 0.21 a	2.02 ± 0.29 ab	4.75 ± 0.09 a

Note: CK (none inundation, 175–180m); SI (short-term inundation, 172–175 m); MI (moderate inundation, 156–172 m); and LI (long-term inundation, 145–156 m). Values are means ± standard deviations (n = 9). Different letters (a and b) in each column indicate significant differences among the four sampling transects at the $p < 0.05$ level (LSD).

3.3. Size Distribution of Water-Stable Aggregates

The effects of the hydrological regime on the water-stable aggregate size distribution were assessed using wet-sieving methods and the results are illustrated in Table 4. The mass percentages of the water-stable macro-aggregates (i.e., aggregates greater than 0.25 mm) at the four sampling transects were more than 73.18%. Among the six size classes, the highest mass percentage of LI (26.83%) was observed in the <0.25 mm fraction, while those of MI (64.29%), SI (68.35%), and CK (77.35%) were found in the > 5 mm fraction. Meanwhile, the differences in the mass percentage of the >5 mm fraction among the sampling transects were significant. As for the proportions of the 5–2 mm and 2–1 mm aggregates, there was a clear increasing trend as the elevation gradient decreased from CK to LI, with increasing proportions of 6% and 9%, respectively. Nevertheless, no significant differences were found among MI, SI, and CK ($p > 0.05$), while the differences between LI and the other three groups were significant ($p < 0.05$). Additionally, compared to CK, the proportion of the 1–0.5 mm aggregates for SI, MI, and LI significantly increased by 12.62%, 92.88%, and 434.95%, respectively. Similarly, both the percentages of the 0.5–0.25 mm aggregates and <0.25 mm micro-aggregates revealed successive increases in the order of CK < SI < MI < LI, and the percentages between LI and the other three groups (MI, SI, and CK) were statistically significant ($p < 0.05$). These results showed that the hydrological regime altered the water-stable aggregate distribution, with a dramatic decline in the larger aggregates and a marked increase in the smaller aggregates.

Table 4. Differential size distribution of water-stable aggregates at four sampling transects in the riparian zone of the TGR.

Sampling Transects	Mass Percentage of Aggregates at Different Sizes (%)					
	>5 mm	5–2 mm	2–1 mm	1–0.5 mm	0.5–0.25 mm	<0.25 mm
CK	77.35 ± 1.51 a	8.00 ± 0.68 b	3.03 ± 0.30 b	2.58 ± 0.33 c	1.80 ± 0.08 b	7.25 ± 0.33 b
SI	68.35 ± 2.11 a	11.73 ± 0.53 b	4.28 ± 0.35 b	4.40 ± 0.48 c	3.30 ± 0.36 ab	7.95 ± 0.70 b
MI	64.29 ± 1.29 b	10.79 ± 0.51 b	5.10 ± 0.28 b	4.97 ± 0.32 b	3.40 ± 0.20 b	11.45 ± 0.62 b
LI	21.91 ± 2.95 c	13.98 ± 1.10 a	11.58 ± 1.05 a	13.78 ± 0.84 a	11.94 ± 1.43 a	26.83 ± 2.92 a

Note: CK (none inundation, 175–180m); SI (short-term inundation, 172–175 m); MI (moderate inundation, 156–172 m); and LI (long-term inundation, 145–156 m). Values are means ± standard deviations (n = 9). Different letters (a, b, and c) in each column indicate significant differences among the four sampling transects at the $p < 0.05$ level (LSD).

3.4. Aggregate Stability along the Elevation Gradient

The soil aggregate stability, indicated by aggregate stability indicators (i.e., MWD, GMD, ASR, and D) and aggregate destruction indexes (i.e., PAD_{MWD} , PAD_{GMD} , PAD_{ASR} , and PAD_D), is presented in Figure 3. On the one hand, the MWD, GMD, and ASR of both the mechanically stable aggregates and water-stable aggregates showed similar successive decreases to the decrease in the elevation gradient, whilst the D_d and D_w changed in the order of CK < SI < MI < LI. Compared to CK, the MWD_d of SI, MI, and LI decreased by

6.60%, 6.67%, and 8.28%, and the MWD_w of SI, MI, and LI dropped by 3.27%, 11.73%, and 54.12%, respectively. Similarly, the GMD_d of SI, MI, and LI declined by 13.07%, 14.89%, and 19.03% in comparison to that of CK, and the GMD_w of SI, MI, and LI went down by 5.61%, 23.73%, and 70.52% in comparison that of CK. Meanwhile, the highest ASR_d (98.78%) and ASR_w (92.75%) appeared in CK, while the ASR_d and ASR_w of LI were the lowest, accounting for 95.25% and 73.18%, respectively. Additionally, the D_d demonstrated successive increments and grew from 1.82 in CK to 2.23 in LI and the D_w increased from 2.41 in CK to 2.63 in LI. On the other hand, the PAD indexes showed a reverse trend to the corresponding aggregate stability indicators. The PAD_{MWD} increased dramatically from 3.12% in CK to 53.20% in LI and the PAD_{GMD} increased from 15.59% in CK to 71.63% in LI. Likewise, the PAD_{ASR} presented a dramatic rise, in that the PAD of LI was approximately four times higher than that of CK. In contrast, the PAD_D gradually declined from 32.08% in CK to 18.17% in LI. Regarding the four indicators of aggregate mechanical stability (i.e., MWD_d , GMD_d , ASR_d , and D_d), there were no significant differences between SI and MI, while significant differences appeared between CK and LI ($p < 0.05$). As for the four indicators of aggregate water stability (i.e., MWD_w , GMD_w , ASR_w , and D_w), there were no significant differences between CK and SI, while the differences were statistically significant between LI and the other three groups ($p < 0.05$). In terms of the aggregate destruction indexes, the PAD_{MWD} , PAD_{ASR} , and PAD_D in LI were significantly different from those in MI, SI, and CK ($p < 0.05$), while an insignificant difference for PAD_{GMD} only appeared between MI and SI. These results indicated that the hydrological regime reduced the aggregate mechanical stability and water stability, and that the longer the inundation lasted, the more unstable the soil aggregates were.

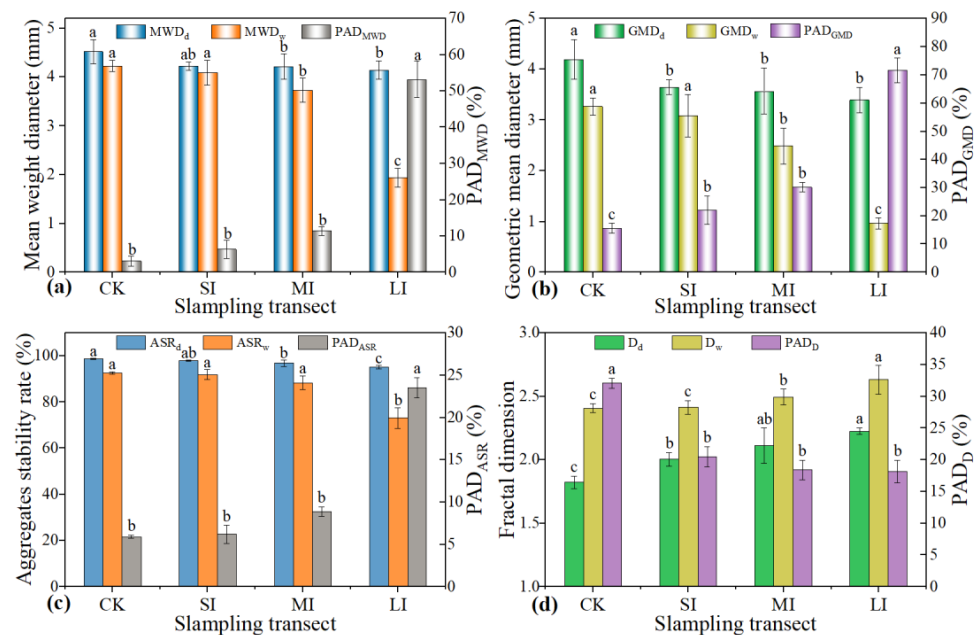


Figure 3. Aggregate stability indicators and aggregate destruction indexes at four sampling transects in the riparian zone of the TGR: (a) mean weight diameter of mechanically stable aggregates and water-stable aggregates and percentage of aggregate destruction of mean weight diameter; (b) geometric mean diameter of mechanically stable aggregates and water-stable aggregates and percentage of aggregate destruction of geometric mean diameter; (c) aggregate stability rate of mechanically stable aggregates and water-stable aggregates and percentage of aggregate destruction of aggregate stability rate; and (d) fractal dimension of mechanically stable aggregates and water-stable aggregates and percentage of aggregate destruction of fractal dimension. CK (none inundation, 175–180 m); SI (short-term inundation, 172–175 m); MI (moderate inundation, 156–172 m); and LI (long-term inundation, 145–156 m). Bars indicate standard deviation. Different letters (a, b, and c) indicate significant differences among four sampling transects at the $p < 0.05$ level (LSD).

3.5. Determinants of Soil Aggregate Stability

A correlation analysis was used to identify the key basic properties influencing the aggregate stability. As shown in Figure 4, a significant or extremely significant correlation existed between the aggregate stability indicators and soil basic properties (sand, silt, clay, BD, and SOC) ($p < 0.05$ or $p < 0.01$). The MWD, GMD, and ASR of both the mechanically stable aggregates and water-stable aggregates were negatively and significantly correlated with sand and BD, whereas there were remarkably positive correlations between these indicators and silt, clay, and SOC. Compared to the correlations above, both D_d and D_w showed a reverse significant correlation with the soil properties. On the other hand, there were statistically significant correlations between the aggregate destruction indexes (i.e., PAD_{MWD} , PAD_{GMD} , PAD_{ASR} , and PAD_D) and the soil properties. The PAD_{MWD} , PAD_{GMD} , and PAD_{ASR} were positively correlated with sand and BD, whilst these indexes were negatively correlated with silt, clay, and SOC. Additionally, the correlations between the PAD_D and soil composition (i.e., sand, silt, and clay) were statistically insignificant ($p > 0.05$), while the significant correlation coefficients between the PAD_D and BD, as well as the SOC, were -0.63 and 0.55 , respectively. Except for a significant correlation between the SOC and PAD_D , an extremely significant correlation appeared between the SOC and the other aggregate stability indicators and aggregate destruction indexes. These results demonstrated that the soil composition, bulk density, and soil organic carbon had significant effects on the aggregate stability, and that the SOC was the most important factor controlling this aggregate stability.

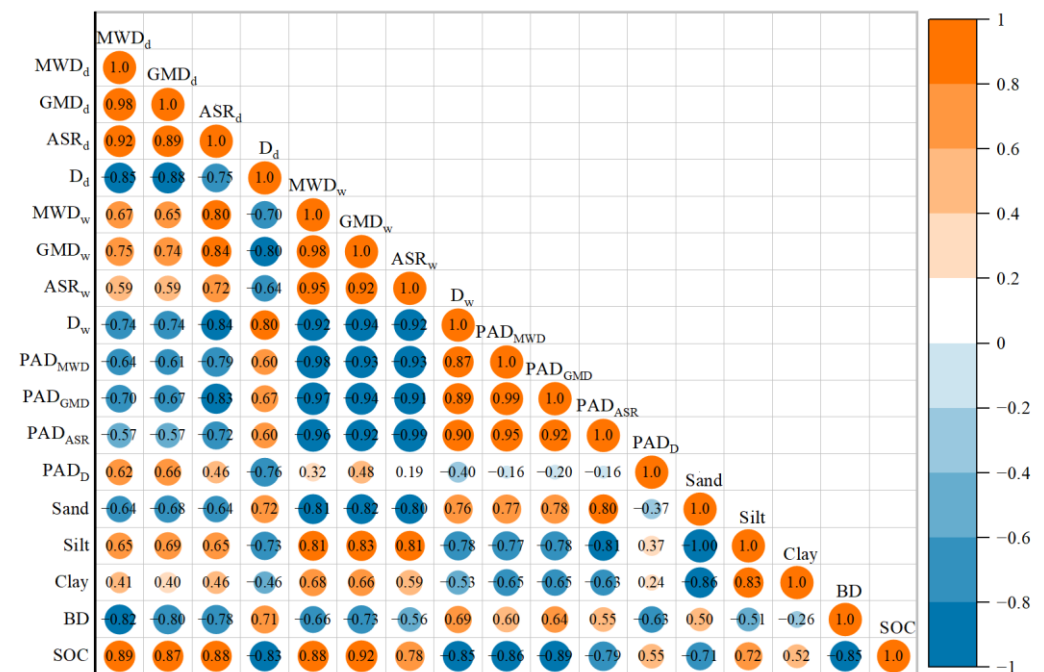


Figure 4. Correlation analysis between soil basic properties and aggregate stability. MWD_d and MWD_w are mean weight diameters of mechanically stable and water-stable aggregates, respectively; GMD_d and GMD_w are geometric mean diameters of mechanically stable and water-stable aggregates, respectively; ASR_d and ASR_w are the mass proportions of the mechanically stable and water-stable aggregates larger than 0.25 mm; D_d and D_w are fractal dimensions of mechanically stable and water-stable aggregates; PAD_{MWD}, PAD_{GMD}, PAD_{ASR}, and PAD_D are percentages of aggregate destruction of MWD, GMD, ASR, and D; BD, bulk density; and SOC, soil organic carbon. The orange color means positive correlation, while the blue color means negative correlation; the lighter color and smaller circle means a lower correlation coefficient, while the darker color and bigger circle means a higher correlation coefficient.

4. Discussion

The hydrological regime is the main factor that drives the various hydrogeomorphic processes affecting the riparian habitat, vegetation diversity, and aggregate stability in a riparian zone [39,40]. Due to the altered hydrological regime of the TGR, the soils in the riparian zone suffer from special anti-seasonal inundation and exposure with a diverse duration, frequency, and amplitude of inundation along the elevation gradient (Table 1), resulting in modifications in the soil aggregate size distribution and stability. The data in the present study demonstrated that a higher proportion of coarse aggregates transformed into fine aggregates along the decreased elevation gradient. With a decrease in the elevation gradient, the MWD, GMD, and ASR of both the mechanically stable aggregates and water-stable aggregates, as well as the PAD_D , significantly decreased, whilst the PAD_{MWD} , PAD_{GMD} , PAD_{ASR} , D_d , and D_w dramatically increased. These results indicated that the hydrological regime of the TGR disintegrated the soil aggregates and reduced the aggregate stability. The longer the inundation was, the higher the disaggregation, and a lower aggregate stability was presented.

More precisely, as illustrated in Tables 3 and 4, with a decrease in the elevation gradient, both the mass percentages of the mechanically stable and water-stable aggregates greater than 5 mm gradually reduced, whereas those of the other five classes significantly increased. In particular, a considerable increase in the mass percentages was present in LI for the water-stable micro-aggregates (i.e., aggregates less than 0.25 mm). Our findings agreed with the previous study conducted by Nsabimana et al. [5]. The results confirmed that large aggregates were more sensitive to the hydrological regime. This is supported by Zhang and Horn [38], who pointed out that the larger an aggregate was, the lower its stability was. Similarly, Hu et al. [41] also demonstrated that aggregates were more prone to disaggregate with an increased initial aggregate size. The alternations in the aggregate size distribution led to a variation in the aggregate stability indicators and aggregate destruction indexes (Figure 3), indicating that the aggregate stability decreased with a decreasing elevation gradient. Similarly, Nsabimana et al. [5] also emphasized the successive aggregate breakdown induced by continuous hydrological stress. However, Ran et al. [26,27] reported that the lowest aggregate stability was presented at the level of strong hydrological stress, while the highest aggregate stability existed at the level of intermediate hydrological stress. Additionally, Cui et al. [17] demonstrated that the highest and lowest aggregate stabilities were under none and intermediate hydrological stresses, respectively. This discrepancy may be attributed to the differences in intrinsic soil properties (e.g., soil composition and soil organic carbon) and external factors such as vegetation distribution and sampling strategy. As mentioned in the introduction, the riparian zone of the TGR has a larger area and a wider extent, contributing to high spatial–temporal heterogeneities in the bedrocks, soil types, topography, and vegetation species in the riparian zone. Unlike the 5 m interval for the sampling transects in the study of Ran et al. [26], our sampling transects were set based on the step-impounded elevation. While Ran et al. [26] sampled Regosols, Anthrosols, and Luvisols from the mainstream and a tributary, our study focused on Regosols in a middled section of the mainstream, causing the contents of silt, clay, and organic carbon in our study to be relatively lower than those of Ran et al. [26], which, in turn, accounted for the distinct aggregate size distribution and stability.

The altered aggregate size distribution and stability in the present study provided evidence of the detrimental effects of the hydrological regime on soil aggregates, which might be ascribed to the changes in the environmental conditions, biotic factors, and soil properties induced by the hydrological regime. Firstly, the hydrological regime has a direct effect on the soil moisture, which can affect the aggregate size distribution and stability [11]. As shown in Figure 2 and Table 1, both the water level and water flow fluctuated with the TGR regulation and rainfall, so the duration, depth, stress, frequency, and amplitude of the inundation increased with a decrease in the elevation gradient. Coupled with the impact of waves and surges by wind and boats, the riparian soils at the lower elevation suffer from severer soaking, elutriation, mellowing, dispersion, and disaggregation. Consequently, the hydrological regime facilitates aggregate hydration and slacking along the decreased

elevation gradient. Secondly, the hydrological regime has direct or indirect impacts on vegetation by altering the temperature, humidity, and oxygen in the soil environment [42–44]. It is commonly accepted that plant roots play an extraordinarily important role in aggregate stability through their penetration, entanglement, decomposition, and root exudates [45,46]. As described in Section 2.2 and Table 1, because of the increasing inundation duration and shorter growing periods with the decreasing elevation, the plant diversity and vegetation cover were progressively reduced. The vegetation in LI was dominated by natural restoration species (e.g., *Cynodon dactylon*), while the vegetation in CK and SI included not only natural restoration species, but also artificial recovery species. Compared to artificial recovery species such as *Hemarthria altissima* and *Paspalum paspaloides*, *Cynodon dactylon* presents the least efficiency for soil reinforcement [47]. Thus, soil aggregates are prone to disintegrate with decreasing elevation. Finally, the above mentioned various external factors may directly or indirectly change the internal soil properties, which are likely to be crucial factors for determining the soil aggregate responses to the hydrological regime [46]. Among soil physicochemical properties, clay and SOC are generally considered as major factors that influence aggregate stability [10,48]. As shown in Figure 4, both the soil texture and SOC had a significant correlation with the aggregate indicators. Compared to the very low and relatively uniform clay content across the hydrological regime, the positive correlation between the SOC and aggregate stability was higher (Figure 4). As a crucial bonding material, the SOC can not only enhance the cohesion between aggregates, but also slow down the wetting rate by forming a hydrophobic layer around soil aggregates [10]. Furthermore, macro-aggregates are stabilized by transient and temporary organic matter, whereas micro-aggregates are cemented by persistent organic matter and organo-mineral complexes, which shows that macro-aggregates are prone to being easily collapsed into stable micro-aggregates under the hydrological regime [46,49]. As reported by Zhong et al. [50], the SOC is closely related to the vegetation species and root distribution in the riparian zone of the TGR. Therefore, the present study showed that the SOC tremendously declined as the elevation decreased (Table 2), which was partly responsible for the enhanced aggregate slacking and reduced aggregate stability with the decreasing elevation gradient. In summary, the present study revealed the combined effects of the hydrological regime on the aggregate size distribution and stability, but the involved mechanisms accounting for these modifications were not discriminated. To better understand and predict soil aggregate changes, the breakdown mechanisms of soil aggregates need to be further investigated.

5. Conclusions

The impacts of the hydrological regime on the soil aggregate size distribution and stability in the riparian zone of the TGR were clarified using dry-sieving and wet-sieving methods. Our results clearly demonstrated that a higher proportion of large aggregates were transformed into small aggregates with an increase in inundation duration, indicating that the hydrological regime disintegrated these soil aggregates and that large aggregates were more sensitive to the hydrological regime. In addition, we also disclosed that, with an increase in inundation duration, the MWD, GMD, ASR, and PAD_D significantly decreased, whilst the PAD_{MWD} , PAD_{GMD} , PAD_{ASR} , and D remarkably increased, suggesting that the hydrological regime reduced the aggregate stability and that the aggregate stability gradually decreased with an increase in the inundation duration. Furthermore, the statistical analysis showed that the differences in the MWD_w , GMD_w , PAD_{GMD} , and D_w were more significant within the elevation gradient than the other indicators, meaning that the MWD_w , GMD_w , PAD_{GMD} , and D_w were more sensitive to the hydrological regime and more suitable for indicating the aggregate stability in this study area. These findings may provide implications for the study of soil erosion in similar riparian zones, but further studies are still needed to focus on the mechanisms of aggregate breakdown and the relationships between aggregate stability and soil erosion.

Author Contributions: Conceptualization, S.Z., X.H. and Y.L.; methodology, S.Z., T.C., X.H. and Y.L.; formal analysis, S.Z. and T.C.; investigation, S.Z., Y.B. and Q.T.; data curation, S.Z., T.C., Y.B. and Q.T.; writing—original draft preparation, S.Z.; writing—review and editing, Y.B., X.H. and Y.L.; visualization, S.Z., T.C., Y.B. and Q.T.; supervision, X.H. and Y.L.; funding acquisition, S.Z., Y.B., Q.T., X.H. and Y.L. All authors have read and agreed to the published version of the manuscript.

Funding: This research was funded by the National Natural Science Foundation of China, grant number 42207385, 41977075, 41771320, U2040207, and the Sichuan Science and Technology Program, grant number 2022YFS0471 and 2020YFQ0002. The APC was funded by 42207385.

Data Availability Statement: Not applicable.

Acknowledgments: The authors would like to thank Mingfeng Wang and Fayou Lü for their assistance in field experiments. The authors thank the editors and anonymous reviewers for their valuable comments and suggestions.

Conflicts of Interest: The authors declare no conflict of interest.

References

- Rabot, E.; Wiesmeier, M.; Schlüter, S.; Vogel, H.J. Soil structure as an indicator of soil functions: A review. *Geoderma* **2018**, *314*, 122–137. [[CrossRef](#)]
- Munkholm, L.J.; Heck, R.J.; Deen, B. Soil pore characteristics assessed from X-ray micro-CT derived images and correlations to soil friability. *Geoderma* **2012**, *181–182*, 22–29. [[CrossRef](#)]
- Le Bissonnais, Y. Aggregate stability and assessment of soil crustability: I. Theory and methodology. *Eur. J. Soil Sci.* **1996**, *47*, 425–437. [[CrossRef](#)]
- Le Bissonnais, Y.; Arrouays, D. Aggregate stability and assessment of soil crustability and erodibility: II. Application to humic loamy soils with various organic carbon contents. *Eur. J. Soil Sci.* **1997**, *48*, 39–48. [[CrossRef](#)]
- Nsabimana, G.; Hong, L.; Yuhai, B.; de Dieu Nambajimana, J.; Jinlin, L.; Ntacyabukura, T.; Xiubin, H. Soil aggregate disintegration effects on soil erodibility in the water level fluctuation zone of the Three Gorges Reservoir, China. *Environ. Res.* **2023**, *217*, 114928. [[CrossRef](#)] [[PubMed](#)]
- Rohošková, M.; Valla, M. Comparison of two methods for aggregate stability measurement—A review. *Plant Soil Environ.* **2004**, *50*, 379–382. [[CrossRef](#)]
- Saygin, S.D.; Cornelis, W.M.; Erpul, G.; Gabriels, D. Comparison of different aggregate stability approaches for loamy sand soils. *Appl. Soil Ecol.* **2012**, *54*, 1–6. [[CrossRef](#)]
- Seybold, C.; Herrick, J. Aggregate stability kit for soil quality assessments. *Catena* **2001**, *44*, 37–45. [[CrossRef](#)]
- Barthès, B.; Roose, E. Aggregate stability as an indicator of soil susceptibility to runoff and erosion; validation at several levels. *Catena* **2002**, *47*, 133–149. [[CrossRef](#)]
- Wu, X.; Wei, Y.; Wang, J.; Wang, D.; She, L.; Wang, J.; Cai, C. Effects of soil physicochemical properties on aggregate stability along a weathering gradient. *Catena* **2017**, *156*, 205–215. [[CrossRef](#)]
- Cosentino, D.; Chenu, C.; Le Bissonnais, Y. Aggregate stability and microbial community dynamics under drying–wetting cycles in a silt loam soil. *Soil Biol. Biochem.* **2006**, *38*, 2053–2062. [[CrossRef](#)]
- Utomo, W.; Dexter, A. Changes in soil aggregate water stability induced by wetting and drying cycles in non-saturated soil. *J. Soil Sci.* **1982**, *33*, 623–637. [[CrossRef](#)]
- Hochman, D.; Dor, M.; Mishael, Y. Diverse effects of wetting and drying cycles on soil aggregation: Implications on pesticide leaching. *Chemosphere* **2021**, *263*, 127910. [[CrossRef](#)] [[PubMed](#)]
- Peng, X.; Hallett, P.D.; Zhang, B.; Horn, R. Physical response of rigid and non-rigid soils to analogues of biological exudates. *Eur. J. Soil Sci.* **2011**, *62*, 676–684. [[CrossRef](#)]
- Rahman, M.T.; Guo, Z.C.; Zhang, Z.B.; Zhou, H.; Peng, X.H. Wetting and drying cycles improving aggregation and associated C stabilization differently after straw or biochar incorporated into a Vertisol. *Soil Tillage Res.* **2018**, *175*, 28–36. [[CrossRef](#)]
- Tang, Q.; Collins, A.L.; Wen, A.; He, X.; Bao, Y.; Yan, D.; Long, Y.; Zhang, Y. Particle size differentiation explains flow regulation controls on sediment sorting in the water-level fluctuation zone of the Three Gorges Reservoir, China. *Sci. Total Environ.* **2018**, *633*, 1114–1125. [[CrossRef](#)]
- Cui, J.; Tang, X.; Zhang, W.; Liu, C. The Effects of Timing of Inundation on Soil Physical Quality in the Water-Level Fluctuation Zone of the Three Gorges Reservoir Region, China. *Vadose Zone J.* **2018**, *17*, 180043. [[CrossRef](#)]
- Bao, Y.; He, X.; Wen, A.; Gao, P.; Tang, Q.; Yan, D.; Long, Y. Dynamic changes of soil erosion in a typical disturbance zone of China's Three Gorges Reservoir. *Catena* **2018**, *169*, 128–139. [[CrossRef](#)]
- Bao, Y.; Yu, D.; Tang, Q.; He, X.; WEI, J.; Hu, Y.; Li, J. Combined Effects of Hillslope-Concentrated Flows and Riverine Stream Waves on Soil Erosion in the Reservoir Riparian Zone. *Water* **2021**, *13*, 3465. [[CrossRef](#)]
- Tang, Q.; Bao, Y.; He, X.; Fu, B.; Collins, A.L.; Zhang, X. Flow regulation manipulates contemporary seasonal sedimentary dynamics in the reservoir fluctuation zone of the Three Gorges Reservoir, China. *Sci. Total Environ.* **2016**, *548–549*, 410–420. [[CrossRef](#)]

21. Bao, Y.; Gao, P.; He, X. The water-level fluctuation zone of Three Gorges Reservoir—A unique geomorphological unit. *Earth Sci. Rev.* **2015**, *150*, 14–24. [[CrossRef](#)]
22. Pires, L.F.; Auler, A.C.; Roque, W.L.; Mooney, S.J. X-ray microtomography analysis of soil pore structure dynamics under wetting and drying cycles. *Geoderma* **2020**, *362*, 114103. [[CrossRef](#)]
23. Amézketa, E. Soil Aggregate Stability: A Review. *J. Sustain. Agric.* **1999**, *14*, 83–151. [[CrossRef](#)]
24. Hussein, J.; Adey, M. Changes in microstructure, voids and b-fabric of surface samples of a Vertisol caused by wet/dry cycles. *Geoderma* **1998**, *85*, 63–82. [[CrossRef](#)]
25. Peng, X.; Horn, R.; Smucker, A. Pore Shrinkage Dependency of Inorganic and Organic Soils on Wetting and Drying Cycles. *Soil Sci. Soc. Am. J.* **2007**, *71*, 1095–1104. [[CrossRef](#)]
26. Ran, Y.; Ma, M.; Liu, Y.; Zhou, Y.; Sun, X.; Wu, S.; Huang, P. Hydrological stress regimes regulate effects of binding agents on soil aggregate stability in the riparian zones. *Catena* **2021**, *196*, 104815. [[CrossRef](#)]
27. Ran, Y.; Ma, M.; Liu, Y.; Zhu, K.; Yi, X.; Wang, X.; Wu, S.; Huang, P. Physicochemical determinants in stabilizing soil aggregates along a hydrological stress gradient on reservoir riparian habitats: Implications to soil restoration. *Ecol. Eng.* **2020**, *143*, 105664. [[CrossRef](#)]
28. Nsabimana, G.; Bao, Y.; He, X.; Nambajimana, J.d.D.; Wang, M.; Yang, L.; Li, J.; Zhang, S.; Khurram, D. Impacts of Water Level Fluctuations on Soil Aggregate Stability in the Three Gorges Reservoir, China. *Sustainability* **2020**, *12*, 9107. [[CrossRef](#)]
29. Nsabimana, G.; Bao, Y.; He, X.; Nambajimana, J.d.D.; Yang, L.; Li, J.; Uwiringiyimana, E.; Nsengumuremyi, P.; Ntacyabukura, T. Soil aggregate stability response to hydraulic conditions in water level fluctuation zone of the Three Gorges Reservoir, China. *Catena* **2021**, *204*, 105387. [[CrossRef](#)]
30. He, X.; Bao, Y.; Nan, H.; Xiong, D.; Wang, L.; Liu, Y.; Zhao, J. Tillage pedogenesis of purple soils in southwestern China. *J. Mt. Sci.* **2009**, *6*, 205–210. [[CrossRef](#)]
31. Zhang, S.-J.; Tang, Q.; Bao, Y.-H.; He, X.-B.; Tian, F.-X.; Lü, F.-Y.; Wang, M.-F.; Anjum, R. Effects of seasonal water-level fluctuation on soil pore structure in the Three Gorges Reservoir, China. *J. Mt. Sci.* **2018**, *15*, 2192–2206. [[CrossRef](#)]
32. Yoder, R. A direct method of aggregate analysis of soils and a study of the physical natural of erosion losses. *J. Am. Soc. Agron.* **1936**, *28*, 337–351. [[CrossRef](#)]
33. Kemper, W.; Rosenau, R. Aggregate Stability and Size Distribution. In *Methods of Soil Analysis, Part 1: Physical and Mineralogical Methods*; Klute, A., Ed.; ASA and SSA: Madison, WI, USA, 1986; pp. 425–442.
34. Zheng, T.; Yang, J.; Zhang, J.; Tang, C.; Liao, K.; Liu, Y. Factors contributing to aggregate stability at different particle sizes in ultisols from Southern China. *J. Soils Sediments* **2018**, *19*, 1342–1354. [[CrossRef](#)]
35. Van Bavel, C. Mean weight-diameter of soil aggregates as a statistical index of aggregation. *Soil Sci. Soc. Am. J.* **1950**, *14*, 20–23. [[CrossRef](#)]
36. Mazurak, A. Effect of gaseous phase on water-stable synthetic aggregates. *Soil Sci.* **1950**, *69*, 135–148. [[CrossRef](#)]
37. Tyler, S.; Wheatcraft, S. Fractal scaling of soil particle-size distribution: Analysis and limitation. *Soil Sci. Soc. Am. J.* **1992**, *56*, 362–369. [[CrossRef](#)]
38. Zhang, B.; Horn, R. Mechanisms of aggregate stabilization in Ultisols from subtropical China. *Geoderma* **2001**, *99*, 123–145. [[CrossRef](#)]
39. Steiger, J.; Tabacchi, E.; Dufour, S.; Corenblit, D.; Peiry, J.L. Hydrogeomorphic processes affecting riparian habitat within alluvial channel-floodplain river systems: A review for the temperate zone. *River Res. Appl.* **2005**, *21*, 719–737. [[CrossRef](#)]
40. Ran, Y.; Wu, S.; Zhu, K.; Li, W.; Liu, Z.; Huang, P. Soil types differentiated their responses of aggregate stability to hydrological stresses at the riparian zones of the Three Gorges Reservoir. *J. Soils Sediments* **2020**, *20*, 951–962. [[CrossRef](#)]
41. Hu, B.; Wang, Y.; Wang, B.; Wang, Y.; Liu, C.; Wang, C. Impact of drying-wetting cycles on the soil aggregate stability of Alfisols in southwestern China. *J. Soil Water Conserv.* **2018**, *73*, 469–478. [[CrossRef](#)]
42. Ye, C.; Butler, O.M.; Chen, C.; Liu, W.; Du, M.; Zhang, Q. Shifts in characteristics of the plant-soil system associated with flooding and revegetation in the riparian zone of Three Gorges Reservoir, China. *Geoderma* **2020**, *361*, 114015. [[CrossRef](#)]
43. Ye, C.; Zhang, K.; Deng, Q.; Zhang, Q. Plant communities in relation to flooding and soil characteristics in the water level fluctuation zone of the Three Gorges Reservoir, China. *Environ. Sci. Pollut. Res. Int.* **2013**, *20*, 1794–1802. [[CrossRef](#)]
44. Zhu, Z.; Chen, Z.; Li, L.; Shao, Y. Response of dominant plant species to periodic flooding in the riparian zone of the Three Gorges Reservoir (TGR), China. *Sci. Total Environ.* **2020**, *747*, 141101. [[CrossRef](#)] [[PubMed](#)]
45. Bronick, C.J.; Lal, R. Soil structure and management: A review. *Geoderma* **2005**, *124*, 3–22. [[CrossRef](#)]
46. Six, J.; Bossuyt, H.; Degryze, S.; Denef, K. A history of research on the link between (micro)aggregates, soil biota, and soil organic matter dynamics. *Soil Tillage Res.* **2004**, *79*, 7–31. [[CrossRef](#)]
47. Zhong, R.; He, X.; Bao, Y.; Tang, Q.; Gao, J.; Yan, D.; Wang, M.; Li, Y. Estimation of soil reinforcement by the roots of four post-dam prevailing grass species in the riparian zone of Three Gorges Reservoir, China. *J. Mt. Sci.* **2016**, *13*, 508–521. [[CrossRef](#)]
48. Peng, X.; Yan, X.; Zhou, H.; Zhang, Y.Z.; Sun, H. Assessing the contributions of sesquioxides and soil organic matter to aggregation in an Ultisol under long-term fertilization. *Soil Tillage Res.* **2015**, *146*, 89–98. [[CrossRef](#)]

49. Tisdall, J.M.; Oades, J.M. Organic matter and water-stable aggregates in soils. *J. Soil Sci.* **1982**, *33*, 141–163. [[CrossRef](#)]
50. Zhong, R.; Hu, J.; Bao, Y.; Wang, F.; He, X. Soil nutrients in relation to vertical roots distribution in the riparian zone of Three Gorges Reservoir, China. *J. Mt. Sci.* **2018**, *15*, 1498–1509. [[CrossRef](#)]

Disclaimer/Publisher’s Note: The statements, opinions and data contained in all publications are solely those of the individual author(s) and contributor(s) and not of MDPI and/or the editor(s). MDPI and/or the editor(s) disclaim responsibility for any injury to people or property resulting from any ideas, methods, instructions or products referred to in the content.